ORIGINAL PAPER

Nagoya J. Med. Sci. **81**. 629–636, 2019
doi:10.18999/nagjms.81.4.629

Factors influencing blood flow resistance from a large internal carotid artery aneurysm revealed by a computational fluid dynamics model

Tasuku Imai[1], Takashi Izumi[1], Haruo Isoda[2,3], Kenta Ishiguro[3], Takashi Mizuno[3], Tetsuya Tsukada[1], Asuka Kropp[1], Masashi Ito[1], Masahiro Nishihori[1], Mamoru Ishida[1], Yosuke Tamari[1], and Toshihiko Wakabayashi[1]

[1]*Department of Neurosurgery, Nagoya University Graduate School of Medicine, Nagoya, Japan*
[2]*Brain and Mind Research Center, Nagoya University, Nagoya, Japan*
[3]*Department of Radiological and Medical Laboratory Sciences, Nagoya University Graduate School of Medicine, Nagoya, Japan*

ABSTRACT

Hyperperfusion syndrome occurs after treatment of a large or giant cerebral aneurysm. Recently, flow-diverter stent placement has emerged as an effective treatment method for a large cerebral aneurysm, but postoperative ipsilateral delayed intraparenchymal hemorrhage occurs in a minority of cases. The mechanism underlying delayed intraparenchymal hemorrhage is not established, but one possibility is hyperperfusion syndrome. The incidence of delayed intraparenchymal hemorrhage appears to be higher for giant aneurysms; hence, we speculated that large/giant aneurysms may create flow resistance, and mitigation by flow-diverter stent deployment leads to hyperperfusion syndrome and delayed intraparenchymal hemorrhage. The purpose of this study was to identify aneurysm characteristics promoting flow resistance by the analysis of pressure loss in an internal carotid artery paraclinoid aneurysm model using computational fluid dynamics. A virtual U-shaped model of the internal carotid artery siphon portion was created with a spherical aneurysm of various angles, body diameters, and neck diameters. Visualization of streamlines, were calculated of pressure loss between proximal and distal sides of the aneurysm, and vorticity within the aneurysm were calculated. The pressure loss and vorticity demonstrated similar changes according to angle, peaking at 60°. In contrast, aneurysm diameter had little influence on pressure loss. Larger neck width, however, increases pressure loss. Our model predicts that aneurysm location and neck diameter can increase the flow resistance from a large internal carotid artery aneurysm. Patients with large aneurysm angles and neck diameters may be at increased risk of hyperperfusion syndrome and ensuing delayed intraparenchymal hemorrhage following flow-diverter stent treatment.

Keywords: large internal carotid artery aneurysm, computational fluid dynamics, pressure loss

Abbreviations:
CFD: computational fluid dynamics
DIPH: delayed intraparenchymal haemorrhage
HPS: hyperperfusion syndrome
ICA: internal carotid artery

Received: January 4, 2019; accepted: March 13, 2019

Corresponding Author: Takashi Izumi, MD, PhD
Department of Neurosurgery, Nagoya University Graduate School of Medicine, 65 Tsurumai-cho, Showa-ku, Nagoya, Aichi 503-8502, Japan
Tel: +81-52-744-2353, Fax: +81-52-744-2360, E-mail: my-yuzu@med.nagoya-u.ac.jp

INTRODUCTION

Cerebral hyperperfusion syndrome (HPS) is caused by rapidly increased blood flow into chronically hypoperfused parenchyma with resultant impaired autoregulation.[1,2] It is a relatively infrequent but potentially severe complication following carotid artery stenting and large cerebral aneurysm treatment.[3-7]

Flow-diverter stent placement is an effective treatment method for large or giant cerebral aneurysms located on the proximal side of the posterior communicating artery (e.g., internal carotid artery [ICA] paraclinoid or cavernous segment), and therefore has gained widespread acceptance in recent years.[8,9] This treatment can preserve the parent artery using one or multiple stents and can promote aneurysm thrombosis or shrinkage, thereby preventing cerebral aneurysm rupture and improving cranial nerve palsy, especially that associated with eye movement. However, delayed intraparenchymal hemorrhage (DIPH) not associated with aneurysm rupture occurs in 2.4%–4.6% of cases following flow-diverter stent deployment, and this complication represents a significant potential limitation to its application.[8-10] The mechanism underlying DIPH is unknown, but one possible candidate is HPS. The incidence of DIPH appears to be higher following stent deployment for giant aneurysms than for smaller aneurysms.[11] Therefore, we hypothesized that large or giant aneurysms may create flow resistance, and reducing this resistance by flow-diverter stent deployment leads to HPS. Therefore, we investigated the features of large cerebral artery aneurysms that enhance flow resistance by creating various computational fluid dynamics (CFD) models of the ICA with large aneurysms at the siphon region.

MATERIALS AND METHODS

Model

A virtual U-shaped ICA vessel model was created with a spherical aneurysm at the siphon portion using the commercially available three-dimensional (3D) formation software 123 Design (Audodesk, San Rafael, CA). The ICA diameter was set to 5 mm, the straight length to 120 mm, and the siphon diameter to 15 mm (Fig. 1a), and the stick angle, size, or neck diameter of the aneurysm was varied. In angle models, the aneurysm size (15 mm) and neck diameter (7.5 mm) were fixed, and the angle was changed from 0° to 180° in 30° increments (seven models). In aneurysm size models, the angle (60°) and neck diameter (7.5 mm) were fixed, and the aneurysm size was changed (10, 15, and 20 mm). In neck diameter models, the angle (60°) and aneurysm size (15 mm) were fixed, and the neck size was varied (6, 7.5, and 10 mm).

Computational Fluid Dynamics

The mesh size minimum and maximum were 0.1 mm and 0.3 mm, respectively. At the boundary layers adjoining the vascular walls, four prism layer meshes were created with an outermost layer thickness of 0.04 mm. CFD calculations were performed using ANSYS CFX version 14.5 (Cybernet Systems Co., Ltd, Tokyo, Japan). We assumed that the circulating fluid is Newtonian and incompressible, with a specific density of 1054 kg/m^3 and a viscosity of 3.8 mPa·s. A rigid wall with no-slip boundary conditions was applied. A pulsatile physiological flow waveform measured in the ICA of physically healthy volunteers using 3D cine phase-contrast magnetic resonance (MR) imaging was used to impose boundary conditions at the inlet, and a pressure boundary condition of P = 0 was applied at the outlet. Two cardiac cycles were simulated, and

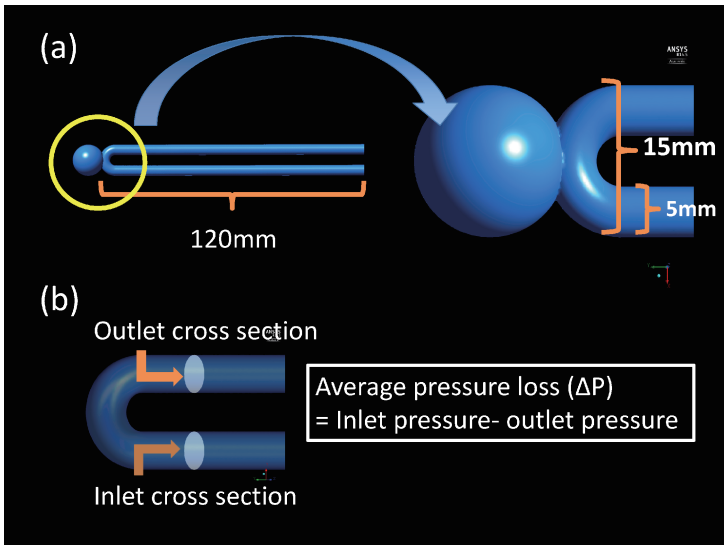

Fig. 1 Diagrammatic representations of the virtual internal carotid artery (ICA) model with a spherical aneurysm
(a) The ICA diameter is 5 mm, the length of the straight portion is 120 mm, and the siphon diameter is 15 mm. (b) Fixed inlet and outlet cross-sections are assumed. The pressure loss between the inlet and outlet for each time phase and the average pressure loss over one cardiac cycle are calculated.

we used the second cycle as the result for each model. Systolic streamlines were calculated and are displayed as color contour images.

Evaluation

We adopted systolic streamlines as representative of the flow stream in each model because they effectively visualize the complex dynamic flow into the vessel and aneurysm. The vorticity in each aneurysm was calculated over one cardiac cycle by vorticity equations using the same CFD software. The vorticity in an aneurysm indicates the complexity of the flow stream. We assumed a fixed inlet and outlet (Fig. 1b) and calculated the pressure loss between the inlet and outlet in each time phase as well as the average pressure loss over one cardiac cycle. The average pressure loss and vorticity over one cardiac cycle were compared among models of a specific type (angle, size, and neck) and to the model constructed with identical conditions except for the aneurysm (no-aneurysm model).

RESULTS

Streamlines, the vorticity in each aneurysm, and pressure loss were obtained in all the ICA plus aneurysm models distinguished by different aneurysm angles (0°–180° in 30° increments) with constant size and neck width (15 mm and 7.7 mm) (Fig. 2), aneurysm sizes (10, 15, and 20 mm) with fixed angle and neck width (60° and 7.5 mm) (Fig. 3), and neck diameters (6, 7.5, and 10 mm) with fixed angle and body size (60° and 15 mm) (Fig. 4). There was almost no difference in pressure loss between the 0° aneurysm model (97.7 Pa) and the non-aneurysm model (96.1 Pa). The highest average pressure loss was found in the 60° model (128.2 Pa). Among the angle models, the changes in average pressure loss and vorticity exhibited similar

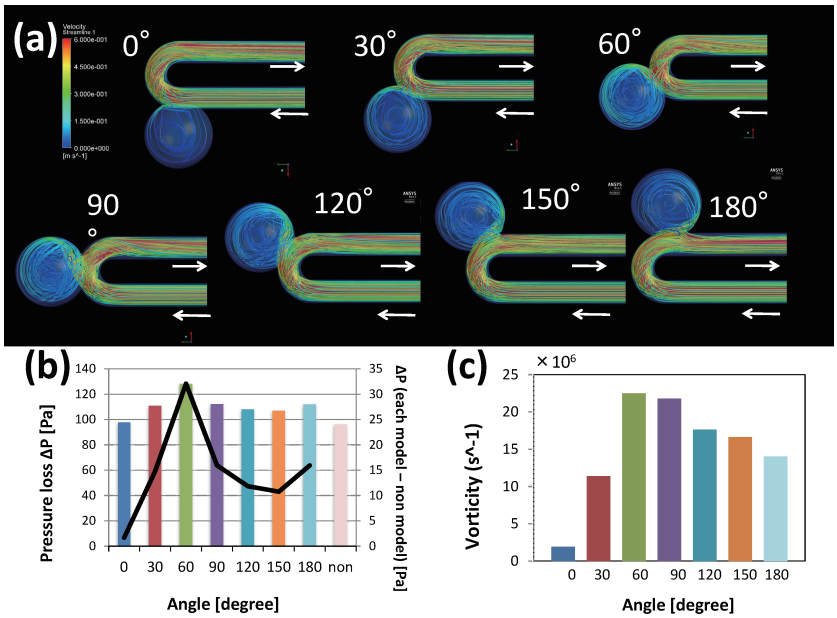

Fig. 2 Results of various angle aneurysm models

Streamlines of the systolic phase (a), graph of pressure loss and difference in average pressure loss between the indicated model and the no-aneurysm model (b), and graph of vorticity with changing angle (c). The aneurysm diameter (15 mm) and the neck diameter (7.5 mm, dome/neck ratio: 2) were fixed. (a) The most vertical streamlines into the aneurysm neck are observed for the 60° model. For the 90° and obtuse-angle models, the streamlines into the aneurysm neck are changed because of the siphon curve. Collisions between streamlines passing by the aneurysm and streamlines emerging from the aneurysm are observed around the neck in all the models. (b) The 60° angle results in peak pressure loss. The pressure loss decreases with higher angles but increases again at 180°. (c) The vorticity also peaks at 60° and then decreases progressively.

trends (Fig. 2b, 2c). In contrast, aneurysm size had little influence on average pressure loss at the same neck width and angle (10 mm: 130.3 Pa; 15 mm: 123.0 Pa; 20 mm: 126.2 Pa) (Fig. 3b). The vorticity was lowest in the 15 mm aneurysm model (22.5 × 10^6/s) (Fig. 3c).

Larger neck width increased the complexity of streamlines in the aneurysm (Fig. 4b). Increasing neck width yielded both greater average pressure loss (6 mm: 108.2 Pa; 7.5 mm: 123.1 Pa; 10 mm: 147.4 Pa) and average vorticity (6 mm: 10.96 × 10^6/s; 7.5 mm: 22.48 × 10^6/s; 10 mm: 33.75 × 10^6/s) (Fig. 4c).

Therefore, angle and neck width but not aneurysm size markedly influenced pressure loss and vorticity of flow within the ICA model.

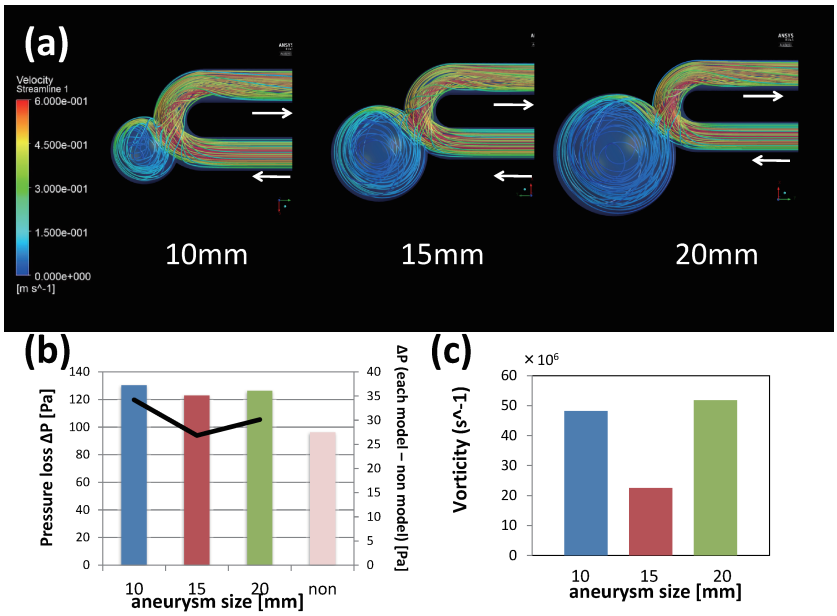

Fig. 3 Results of various aneurysm diameter models
Streamlines of the systolic phase (a), graph of pressure loss and difference in average pressure loss between the indicated model and the no-aneurysm model (b), and graph of vorticity with changing aneurysm diameter (c). The aneurysm angle (60°) and neck diameter (7.5 mm) were fixed. The pressure loss does not change substantially with aneurysm diameter. The vorticity is lowest in the 15 mm aneurysm model.

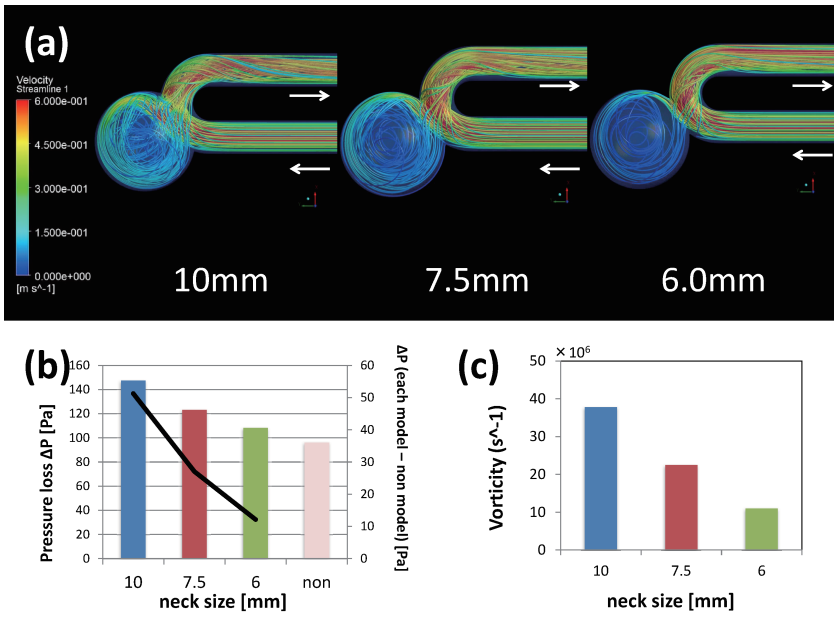

Fig. 4 Results of various aneurysm neck diameter models
Streamlines of the systolic phase (a), graph of pressure loss and difference in average pressure loss between the indicated model and the no-aneurysm model (b), and graph of vorticity with changing neck diameter (c). The aneurysm angle (60°) and diameter (15 mm) were fixed. A larger neck width increases the number of streamlines into the aneurysm, causing greater pressure loss and vorticity.

DISCUSSION

Pressure Loss and Vorticity

The flow rates at the inlet and outlet are the same for each model because of fixed geometry; therefore, total energy loss is proportional to pressure loss. The total pressure loss can be divided into loss across the vessel (ΔPv) and from the proximal to the distal side of the aneurysm (ΔPa), as shown below:

$$\Delta P = \Delta Pv + \Delta Pa \quad (1)$$

The vessel component of pressure loss (ΔPv) is mainly caused by flow separation and friction on the vessel wall. In our models, ΔPv was roughly equivalent; hence, the total pressure loss compared with that of the non-aneurysm model was determined primarily by the specific geometric characteristics of the aneurysm. The vorticity in our models mainly reflects the fact that the complexity of streamlines inside the aneurysm, and the higher vorticity in the aneurysm, indicates greater total energy loss. This is the reason why the vorticity and pressure loss demonstrated similar trends in the angle models (except that the pressure loss was larger at 180° than at 120° or 150°, whereas the vorticity was smaller). In this specific case, the pressure loss across the vessel element (ΔPv) was larger than across the aneurysm element (ΔPa). In contrast to location (angle), the pressure loss was almost the same among the three aneurysm size models, whereas the average vorticity differed. It is speculated that pressure loss across the vessel element (ΔPv), which is mainly due to friction of the vessel wall, and the collision of aneurysm in- and out-streams strongly influence the total pressure loss (ΔP). Furthermore, greater neck width increased both vorticity and pressure loss across the aneurysm. Therefore, both aneurysm location and neck size were associated with pressure loss. Pressure loss and vorticity are distinct physical entities. However, in this model with fixed vessel conditions, similar trends were observed because vorticity within the aneurysm accounted for most of the pressure drop (i.e., energy loss).

DIPH and HPS

Flow-diverter stents are relatively new devices for the treatment of intracranial large or giant aneurysms. The placement of flow-diverter stents promotes thrombosis and shrinkage within the aneurismal sac, preventing rupture and improving cranial nerve palsy.[10] The periprocedural and mid-term follow-up results of this treatment have been impressive, with a high rate of complete occlusion of the aneurysm and relatively low rates of morbidity and mortality.[10,12] However, the rate of DIPH not associated with aneurysm rupture after flow-diverter stent deployment is 2.4%–4.6%, representing a significant potential limitation of this treatment strategy.[8-10] The mechanism for DIPH is not established, but proposed explanations include hemorrhagic transformation of ischemic stroke,[13] HPS,[4] dual antiplatelet therapy or P2Y12 receptor overinhibition,[14] and hemodynamic alterations.[11,12] According to a recent review, most cases of DIPH appear within the first week (less than 1 day in 24% and 1–7 days in 42% of cases) and the vast majority within 1 month (86%).[11] However, it has proven difficult to predict risk from these findings, possibly because of the unpredictability of thrombosis in the aneurysm sac.[10,12]

Several factors likely contribute to DIPH. Our modeling results suggest that a large or giant aneurysm can induce substantial pressure loss, resulting in HPS after flow-diverter stent deployment. According to these modeling results, aneurysm location and neck size are the main factors accounting for pressure loss across the aneurysm. It is possible that calculation of pressure loss across the aneurysm using CFD before stent deployment may be useful for predicting DIPH risk, especially using CFD simulations in which vascular geometry is obtained by 3D computed tomography or 3D rotation angiography and patient-specific boundary conditions are obtained

from 3D cine phase-contrast MR imaging.[17,18]

Limitations

This study has a number of limitations. The actual ICA has branches, tortuosity, variable arteriosclerosis or stenosis, and a more complex siphon shape than our U-shaped model. These factors may influence the pressure loss, but we focused only on aneurysm geometry. Moreover, our virtual model includes a rigid wall condition, which is unlike a human vessel. Further experiments are necessary to examine how these factors affect pressure loss.

CONCLUSION

In vitro analyses of the geometric characteristics of large ICA aneurysms in the siphon portion indicate that the location (angle) and neck diameter are major influences on flow resistance and pressure loss. Removal of this pressure loss by stent deployment may lead to HPS, which in turn is a possible contributing factor to ipsilateral DIPH. If so, applying this computational method for the calculation of pressure loss between the proximal and distal sides of a large aneurysm before flow-diverter stent deployment may help in predicting the risk of DIPH.

ACKNOWLEDGEMENTS

The authors thank Yasumasa Ito, Ph.D., and Yasuhiko Sakai, Ph.D. (Department of Mechanical Systems Engineering, Nagoya University), for their valuable insights in theoretical physics.

DISCLOSURE STATEMENT

This research did not receive any specific grant from funding agencies in the public, commercial, or not-for-profit sectors. The authors report no conflicts of interest.

REFERENCES

1) Narita S, Aikawa H, Nagata S, et al. Intraprocedural prediction of hemorrhagic cerebral hyperperfusion syndrome after carotid artery stenting. *J Stroke Cerebrovasc Dis*. 2013;22(5):615–619.
2) Lieb M, Shah U, Hines GL. Cerebral hyperperfusion syndrome after carotid intervention: a review. *Cardiol Rev*. 2012;20(2):84–89.
3) Ecker RD, Murray RD, Seder DB. Hyperperfusion syndrome after stent/coiling of ruptured carotid bifurcation aneurysm. *Neurocrit Care*. 2013;18(1):54–58. doi: 10.1007/s12028-012-9733-x.
4) Chiu AH, Wenderoth J. Cerebral hyperperfusion after flow diversion of large intracranial aneurysms. *BMJ Case Rep*. 2012;15:pii: bcr2012010479.
5) Murakami H, Inaba M, Nakamura A, Ushioda T. Ipsilateral hyperperfusion after neck clipping of a giant internal carotid artery aneurysm. *Case report. J Neurosurg*. 2002;97(5):1233–1236.
6) Maruya J, Nishimaki K, Minakawa T. Hyperperfusion syndrome after neck clipping of a ruptured aneurysm on a dolichoectatic middle cerebral artery. *J Stroke Cerebrovasc Dis*. 2011;20(3):260–263.
7) Kayahara T, Takeda R, Kikkawa Y, Take Y, Kurita H. Hyperperfusion syndrome after aneurysm surgery: a case report. *Acta Neurochir*. 2015;157(11):1855–1857.
8) Kallmes DF, Hanel R, Lopes D, et al. International retrospective study of the pipeline embolization device: a multicenter aneurysm treatment study. *AJNR Am J Neuroradiol*. 2015;36(1):108–115.
9) Brinjikji W, Murad MH, Lanzino G, Cloft HJ, Kallmes DF. Endovascular treatment of intracranial aneurysms with flow diverters: a meta-analysis. *Stroke*. 2013;44(2):442–447. doi: 10.1161/STROKEAHA.112.678151.

10) Becske T, Kallmes DF, Saatci I, et al. Pipeline for uncoilable or failed aneurysms: results from a multicenter clinical trial. *Radiology*. 2013;267(3):858–868.
11) Rouchaud A, Brinjikji W, Lanzino G, Cloft HJ, Kadirvel R, Kallmes DF. Delayed hemorrhagic complications after flow diversion for intracranial aneurysms: a literature overview. *Neuroradiology*. 2016;58(2):171–177.
12) Becske T, Brinjikji W, Potts MB, et al. Long-Term clinical and angiographic outcomes following pipeline embolization device treatment of complex internal carotid artery aneurysms: five-year results of the pipeline for uncoilable or failed aneurysms trial. *Neurosurgery*. 2017;80(1):40–48.
13) Shannon P, Billbao JM, Marotta T, Terbrugge K. Inadvertent foreign body embolization in diagnostic and therapeutic cerebral angiography. *AJNR Am J Neuroradiol*. 2006;27(2):278–282.
14) Almandoz JE, Crandall BM, Scholz JM, et al. Pre-procedure P2Y12 reaction units value predicts perioperative thromboembolic and hemorrhagic complications in patients with cerebral aneurysms treated with the Pipeline Embolization Device. *J Neurointerv Surg*. 2013;5(suppl 3):iii3–10.
15) Cruz JP, Chow M, O'Kelly C, et al. Delayed ipsilateral parenchymal hemorrhage following flow diversion for the treatment of anterior circulation aneurysms. *AJNR Am J Neuroradiol*. 2012;33(4):603–608.
16) Cebral JR, Mut F, Raschi M, et al. Aneurysm rupture following treatment with flow-diverting stents: computational hemodynamics analysis of treatment. *AJNR Am J Neuroradiol*. 2011;32(1):27–33.
17) Isoda H, Ohkura Y, Kosugi T, et al. In vivo hemodynamic analysis of intracranial aneurysms obtained by magnetic resonance fluid dynamics (MRFD) based on time-resolved three-dimensional phase-contrast MRI. *Neuroradiology*. 2010;52(10):921–928.
18) Watanabe T, Isoda H, Takehara Y, et al. Hemodynamic vascular biomarkers for initiation of paraclinoid internal carotid artery aneurysms using patient-specific computational fluid dynamic simulation based on magnetic resonance imaging. *Neuroradiology*. 2018;60(5):545–555.